The International Journal Of Engineering And Science (IJES)
||Volume||2 ||Issue|| 4 ||Pages|| 66-79||2013||
ISSN(e): 2319 – 1813 ISSN(p): 2319 – 1805

Thermal Aspect of Machining: Evaluation of Tool and Chip Temperature during Machining Process Using Numerical Method.

[1,]Uzorh Augustine .C and [2,]Nwufo Olisaemeka .C
[1,2,]*Department Of Mechanical Engineering, Federal University Of Technology P.M.B. 1526 Owerri, Imo State, Nigeria*

----------Abstract----------

Elevated temperatures generated in machining operations significantly influence the chip formation mechanics, the process efficiency and the surface quality of the machine parts. The temperature fields generated in the cutting process are subject of extensive research. The studies of these thermal fields in machining are very important for the development of new technologies aiming to increase the tool lives and to reduce production costs. Particular attention is given to modeling of the tool-chip, chip-work piece and tool-work piece interfaces. Since the direct temperature measurement at the chip-tool interface are very complex, this work proposes the estimation of the temperature and the heat flux at the chip-tool interface using the inverse heat conduction problem technique. The shear energy created in the primary zone, the friction energy produced at the rake face-chip contact zone and the heat balance between the moving chip and the stationary tool are considered. The temperature distribution is solved using finite difference method. The temperature and flux fields for various machining conditions along with their sensitivities and the situations of progressive flank and crater wear of the tool with continued machining are also considered. The mathematical models and simulation results are in satisfactory agreement with experimental temperature measurements reported in the literature.

Keywords: *Machining; Temperature; Chip-Tool Interface; Heat; Finite Difference*

Date of Submission: 23 Feb 2013 Date Of Publication: 25, April.2013

NOMENCLATURE

α_n, β_n, V	Normal tool rake, normal friction and clearance angles
dx, dy	Grid lengths along the x and y axes
$\delta\psi$	Angular increment of the tool grids
θ	Cutter rotation angle
ρ	Material density
τ, ϕ_n	Shear stress and shear angle in the shear plane
α	Thermal diffusivity
$[A]$	Square coefficient matrix of the chip heat equilibrium equations
χ	Proportion of the shearing heat entering into the workpiece
Γ_i	Proportion of the frictional heat entering into the tool at the *ith* nodal point
c	Feed per revolution in turning, feed per tooth in milling
C_c	Specific heat capacity of the chip
$\{C\}$	Heat generation array in the chip heat equilibrium equations
$[D]$	Square coefficient matrix of the tool heat equilibrium equations
dA	Differential control zone
$\{E\}$	Heat generation array in the tool heat equilibrium equations
F_f	Frictional force
F_s	Shear force
h_c	Instantaneous uncut chip thickness
k_t, k_c	Thermal conductivity of the tool and chip
l_{cn}	Tool–chip contact length
l	Shear plane length

N_p Number of the angular divisions for the cutter meshes in the polar coordinates
N_x, N_y Number of the divisions for the chip meshes along the x, y axis (Fig. 4)
$\dot{Q}$ Heat conduction rates
Q_g Energy generation rate in the control volume (or in the control area in the 2-D)
R_t Thermal number
$\dot{Q}_s, \dot{Q}_f$ Rate of energy generated per unit depth of cut in the shear plane and along the tool–chip contactlength, respectively
r_{max} Radius corresponding to the backside of the tool (at nodal point R)
s Nodal point number (at r_{max}) assigned to the tool on the rake face
$\{T_c\}, \{T_t\}$ Chip and tool temperature arrays
V_w, V_c, V_s Cutting, chip and shear velocities, respectively
h Heat transfer coefficient
C_p Specific heat capacity
$q^{"}$ Heat flux

I. INTRODUCTION

The importance of temperature prediction for the machining processes has been well recognized in the machining research community primarily due to its effects on tool wear and its constraints on the productivity. It is well observed that particularly the rate of wear is greatly dependent on the tool–chip interface temperature Usui et al. (1978). Temperature is one of the major concerns and, after chatter stability, which is the main limitation in the selection of process parameters, such as cutting speed and feedrate, in the machinability and production of some advanced materials such as titanium and nickel-based alloys (Klocke et al 1996). In these materials, due to their low thermal conductivity, most of the heat generated during the machining flows into the tool causing severe thermal stresses on the cutting tool accelerates tool fatigue and failures due to fracture, wear or chipping. Furthermore, if the temperature exceeds the crystal binding limits, the tool rapidly wears due to accelerated loss of bindings between the crystals in the tool material.

Loewen and Shaw (1954) have stated that it is not possible to experimentally determine the influence of many of the variables on the cutting temperature, or to measure conveniently its components. They developed a simple analytical procedure to compute the interface temperature by making the assumptions that the fraction of heat flow into the chip is constant along the rake face in the tool–chip contact region, and the tool acts like a quarter-infinite body. Usui et al. (1978) and Tlusty et al. (1981) used the finite difference method to predict the steady-state temperature distribution in continuous machining by utilizing the predicted quantities, such as chip formation and cutting forces, through the energy method. The predicted temperatures were lower than the observed ones near the cutting edge and the chip leaving point. They correlated the crater wear of carbide tools to the predicted temperature and stresses in the tool. Smith and Armarego (1981) have predicted temperature in orthogonal cutting with a finite difference approach. Ren and Altintas (2000) applied a slip line field solution proposed by Oxley (1989) on high speed orthogonal turning of hardened mold steels with chamfered carbide and CBN tools.

They evaluated the strain, strain rate and temperature dependent flow stress of the material, as well as the friction field at the rake face–chip contact zone from standard orthogonal cutting tests conducted with sharp tools. They showed a good correlation between the maximum temperature on the rake face and crater wear, which led to the identification of cutting speed limits for an acceptable tool life limits. Strenkowski and Moon (1990) have developed an Eulerian finite element model to simulate the cutting temperature. This Eulerian formulation of the cutting model requires a constitutive law between the viscosity, second invariant of the strain rate tensor and uniaxial yield stress. An iterative computational scheme is also required for the solution. Numerical solutions, especially Finite Element (FE) methods require accurate representation of material's constitutive properties during machining. Shatla et al. (1999) used the material properties evaluated from orthogonal cutting and milling tests in the FE simulation of metal cutting. He reported improvements predicting the temperature and cutting forces in both continuous turning and transient milling operations using a Finite Element method.

In this work, the finite difference method is used for the predictions of steady-state tool and chip temperature fields and transient temperature variation in continuous machining and milling. Based on the first law of thermodynamics, heat balance equations are determined in partial differential equation forms for the chip in Cartesian coordinates and for the tool in the polar coordinates. Thereafter, the finite difference method is

utilized for the solutions of the steady-state tool and chip temperature fields. Steady-state chip and tool temperature fields are determined for each of the discretized machining intervals. Based on thermal properties and boundary conditions, time constants are determined for each discrete machining interval. Based on knowledge of the steady-state temperature and time constants of the discretized first order heat transfer system, an algorithm is presented to determine the transient temperature variations. Simulation results for continuous machining processes are presented and compared with the experimental data reported in the literature. These works has used simplified models considering either the geometrical dimensions or steady conditions.

1.1 Heat In Machining

Heat has critical influence on machining; to some extent, it can increase tool wear and then reduce tool life due to thermal deformation and can add to environmental problems. Due to the complexity of machining mechanics, it is hard to predict the intensity and distribution of heat sources in individual machining operations. Especially, because the properties of material used in machining vary with temperature, the mechanical process and the thermal dynamic process are tightly coupled together.

1.2 Heat Generation In Metal Cutting

The heat generated during cutting operation depends on the rate of metal cutting, cutting speed, specific heat and thermal conductivity of the workpiece and tool material. Amongst all these parameters mentioned, cutting speed has more influence on the temperature rise during operation hence heat generated. This is because as speed increases, the time for heat dissipation decreases, thus temperature increases. The total heat generated Q during a machining operation is distributed between workpiece, tool, chips and surrounding.

$$Q_{total} = Q_w + Q_T + Q_c + Q_s \dots\dots\dots\dots\dots\dots 1$$

Where, Q_w, Q_T, Q_C and Q_s is the amount of heat conducted into the workpiece, tool, chips and is the amount of heat dissipated to the surroundings respectively.

The amount of heat dissipated to the surroundings is very small and can be neglected. The heat distributed in metal cutting operation is approximately 80:10:10 between chips, tool and workpiece. This ratio shows that the majority of heat generated during the process is carried away by the chips.

1.3 Heat Generation In Various Machining Operations

Almost all of the heat generation models were established under orthogonal cutting condition. But in practice, there are various machining operations which cannot satisfy that condition, such as oblique turning, boring, drilling, milling, grinding etc.

1.4 Heat Generated In Primary Zone

Heat generated in this zone is mainly due to plastic deformation and viscous dissipation. But in classical machining theory, the rate of heat generated is the product of the shear plane component, F_s, of the resultant force and the shear velocity V_s, i:e the shear energy is completely converted into heat. If heat source is uniformly distributed along the shear plane, the intensity of shear plane heat source, I_p, satisfies the following equation.

$$I_p = \frac{F_s V_s}{b t_1} \dots\dots\dots\dots\dots\dots\dots\dots\dots\dots 2$$

Where b is the cutting width and t_1 the uncut depth

1.5 Heat Generated In Secondary Zone

In this region, because of the complexity of plastic deformation, this part of heat was ignored in many previous theoretical researches. Boothroyd has shown that the secondary plastic zone is roughly triangular in shape and that strain rate, E, in this region varies linearly from an approximately constant value along the tool-chip interface given by

$$E = \frac{V_C}{d_t} \dots\dots\dots\dots\dots\dots\dots\dots\dots\dots 3$$

Where V_c is the chip velocity and d_t the maximum thickness of the zone.

1.6 Heat Generated At The Interface Between Chip And Tool

Heat is generated at tool-chip interface by friction. The intensity, I_c of the frictional heat source is approximately given as

$$I_c = \frac{F V_x}{hb} \dots\dots\dots\dots\dots\dots\dots\dots\dots\dots 4$$

Where F is the friction force, V_x the sliding velocity of the chip along the interface, and h is the plastic contact length.

II. MATERIALS AND METHOD(THERMAL MODEL)

The thermal model of the insert-tool holder assembly, shown in Fig. 1, is described by the transient three-dimensional heat diffusion equation. The equation considering temperature dependent thermal properties can be written as

$$\frac{\partial}{\partial x}\left(K_i\frac{\partial T}{\partial x}\right)+\frac{\partial}{\partial y}\left(K_i\frac{\partial T}{\partial y}\right)+\frac{\partial}{\partial z}\left(K_i\frac{\partial T}{\partial z}\right)=(\rho C_p)_i\frac{\partial T}{\partial t} \dots\dots\dots\dots\dots\dots 5a$$

subjected to the following boundary conditions:

- in the regions exposed to the environment:

$$K_i\frac{\partial T}{\partial \eta}=h(T-T_\infty) \dots\dots\dots\dots\dots 5b$$

- at the chip–tool–workpiece interfaces:

$$K_i\frac{\partial T}{\partial \eta}=q^*(t) \dots\dots\dots\dots\dots\dots\dots 5c$$

- initial condition:

$$T(x,y,z,0)=T_\infty$$

In Eq. (5) T is the temperature, $\frac{\partial T}{\partial \eta}$ the derivative along the outward drawn normal to the surface, α the thermal diffusivity coefficient, K, the thermal conductivity coefficient, ρ the density, C_p the heat capacity, h the heat transfer coefficient at the assembly surface, t the time and T_∞ is the medium temperature.

It should be noted in Fig. 1 that all assembly surfaces are exposed to the environment but the interface contact area, Ap.

As mentioned before, this area is subjected to the heat flux $q^*(t)$ generated due to contact with the tool and the chip, Fig. 1b.

If the value of the heat flux $q^*(t)$ is known, the Eq. (5) represents the direct problem related to the inverse problem studied.

The index i represents the position in the assembly as follows: $i=1$ represents the tool cutting; $i=2$ represents the tool shim and $i=3$ represents the tool holder.

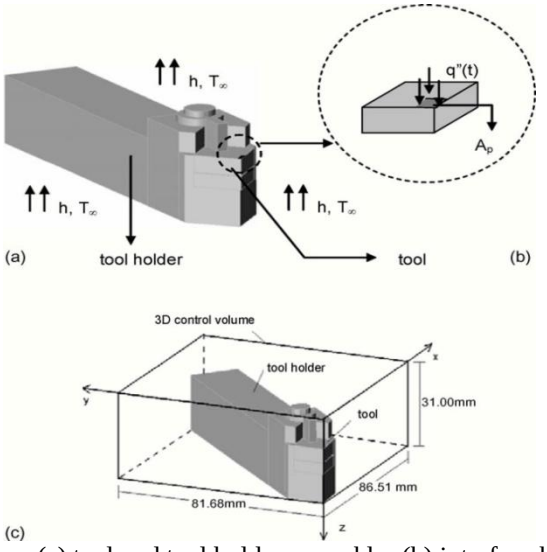

Fig. 1. Thermal problem scheme: (a) tool and tool holder assembly; (b) interface heat flux detail; (c) 3D control volume

As mentioned before, the Eq. (5) is solved using the finite difference technique. The calculation domain is carried out using the control-volume method in which the energy conservation principle is applied directly in a control volume. The implicit approximation scheme is used to step the time derivative of the temperature. Fig. 2 shows the grid mesh.

The discretized equation of Eq. (5) in the context of finite control volume (Patankar 1980) can be expressed as

$$a_0 T_{i,j,k}^{p+1} + a_w T_{i-1,j,k}^{p+1} + a_e T_{i+1,j,k}^{p+1} + a_s T_{i,j-1,k}^{p+1} + a_n T_{i,j+1,k}^{p+1} + a_b T_{i,j,k-1}^{p+1} + a_f T_{i,j,k+1}^{p+1} = b \dots\dots\dots 6$$

where subscripts i, j, k denote the cell location, *p* denotes the value at present time, the coefficients a_0, a_w, a_e, a_s, a_n, a_b, a_f and the source term *b* are the coefficients with geometric and physical contribution. The coefficient expressions can be found in detail at Carvalho (2005). To solve the systems of algebraic equations, Eq. (6), the Gauss–Seidel iteration with the successive over relation method is used (Patankar 1980).

2.1 Heat Flux Estimation, Q(t)

One way to estimate the heat flux q(t), present in Eq. (5),is to require that the traditional least square function, F_q, defined as the error between the computed temperature T_i and the measured temperature, Y_i is minimized with respect to the unknown *q(t)*. F_q is then defined as

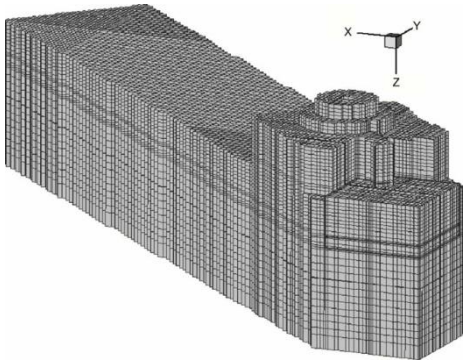

Fig. 2. Non-regular finite volume mesh for the assembly tool, shim and tool holder

$$F_{qm} = \sum_{n=1}^{N} \{Y(r_n, t_m) - T(r_n, t_m, q_m)\}^2 \dots\dots\dots 7$$

where *r* represents the vector position of the rectangular coordinate system *(x, y, z), n* denotes the thermocouple position and m the measurement time.

There are several inverse techniques that can solve this machining problem optimization.). All these techniques use temperature histories experimentally determined in the sample (workpiece) to calculate the corresponding input heat flux for a given set of system parameters.

In this work, in order to minimize the Eq. (7) the Golden Section technique followed by a polynomial approximation is used (Vanderpaats 1995). It means that the values of q_m will be supposed to be those that minimize Eq. (7). This procedure requires that the estimated temperature$T(r_n, t_m, q_m)$, *m=1,2,...,M,* computed from the solution of direct problem, Eq. (5), by using the estimated values of the components q_m, *m =1, 2,..., M,* should match the measured temperature $Y(r_n, t_m)$ as closely as possible for each instant tm. The Golden Section method is a well-known optimization technique to estimated heat flux component in a sequential way.

2.2 Heat Generated In The Primary And Secondary Deformation Zones

It is assumed that the process has orthogonal cutting geometry and the chip is sheared from the blank at an infinitely thin shear plane (i.e. primary deformation zone). The chip slides on the rake face (i.e. secondary deformation zone) with a constant average friction coefficient. Heat generated per unit depth of cut in the primary and secondary zones are given as follows, respectively, [8]

$$\dot{Q}_s = F_s V_s = \frac{\tau h_c V_w \cos(\alpha_n)}{\sin(\emptyset_n)\cos(\emptyset_n - \alpha_n)} \dot{Q}_f = F_f V_c \dots\dots\dots 8$$

$$= \frac{\tau h_c V_w \sin(\beta_n)}{\cos(\emptyset_n + \beta_n - \alpha_n)\sin(\emptyset_n - \alpha_n)}$$

where F_s, F_f, V_w, V_s and V_c are the shear force in the shear plane, the frictional force between the tool rake face and the chip contact zone, the cutting velocity, the cutting velocity component along the shear plane and the cutting velocity component along the rake face, respectively. τ, $\emptyset_n$, α_n and β_n are the shear stress in the shear plane, shear angle, normal rake angle and normal friction angle, respectively. *h* is the instantaneous uncut chip thickness *(h_c=feed per revolution for turning, $h_c = c \sin\theta$ for end-milling, where c is the feed per tooth and θ represents the angular position of the cutting point).*

The average temperature rise of the chip per unit depth of cut due to the shearing is determined by Oxley's energy partition function

$$\Delta\bar{T} = \dot{Q}_s \frac{1-\chi}{\rho C_c h_c V_w} \dots\dots\dots\dots\dots\dots\dots\dots\dots\dots 9$$

Where ρ and C_c are the mass density and specific heat capacity of the chip, respectively. χ represents the proportion of the shearing flux entering into the workpiece, and is defined by:

$$\chi = 0.5 - 0.35\log_{10}(R_t \tan(\emptyset_n)) \quad for\ 0.004 \le R_t \tan(\emptyset_n) \le 10$$

$$\chi = 0.3 - 0.15\log_{10}(R_t \tan(\emptyset_n))$$

$$for\ R_t \tan(\emptyset_n) \ge 10$$

$$(thermal\ number)\ \ R_t = \frac{h_c V_w}{\alpha}, (thermal\ diffusivity)\ \alpha = \frac{K_c}{\rho C_c}.$$

The average temperature rise on the shear plane is used as a boundary condition at Point D in Fig. 4, and the heat generated in the primary and secondary zones are used as heat sources in solving the temperature distribution within the tool and chip as presented in the following section.

2.3 Modeling And Computational Algorithm For Steady-State Chip–Tool Temperature Fields

Based on the first law of thermodynamics, the energy balance in a two-dimensional (2-D) differential control zone can be written in Cartesian coordinates as:

$$\dot{Q}_x + \dot{Q}_y + \dot{Q}.dx.dy - \dot{Q}_{x+dx} - \dot{Q}_{y+dy} = \rho C_p \frac{\partial T}{\partial t}.dx.dy \dots\dots\dots\dots 10$$

Where $dx.dy$ is the area of the infinitesimal element zone, $\dot{Q}, (\dot{Q}_x, \dot{Q}_y)$ and $(\dot{Q}_{x+dx}, \dot{Q}_{y+dy})$ are the energy generation rates per unit area, the heat conduction input and output rates, respectively, which are perpendicular to the each control surface as shown in Fig. 1. ρ, C_p, t, T represent mass density, specific heat capacity of medium, time and the temperature in the element, respectively.

The heat conduction rates $(\dot{Q}_x, \dot{Q}_y)$ can be evaluated from Fourier's Heat Conduction Law,

$$\dot{Q}_x = -k.dy.\frac{\partial T}{\partial x}, \dot{Q}_y = -k.dx.\frac{\partial T}{\partial y} \dots\dots\dots 11$$

Where k is the thermal conductivity of the material.

Using Taylor series expansion and ignoring the higher order terms, the heat flow rates in two orthogonal directions can be written as first order approximations:

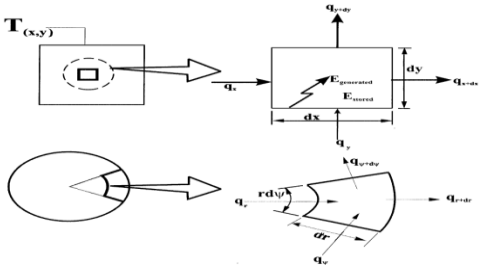

Fig. 3. Heat diffusion in differential control zones defined in Cartesian and Polar Coordinates

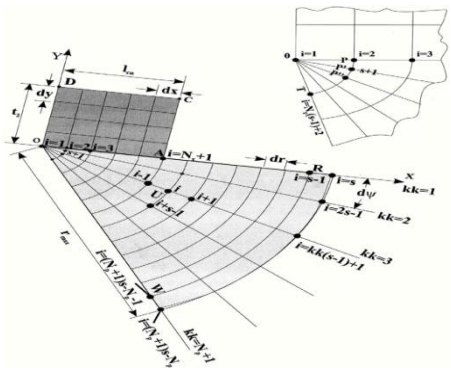

Fig. 4. Illustration of chip and tool meshing

$$\dot{Q}_{x+dx} = \dot{Q}_x + \frac{\partial \dot{Q}_x}{\partial x}dx, \dot{Q}_{y+dy} = \dot{Q}_y + \frac{\partial \dot{Q}_y}{\partial y}d \ldots\ldots\ldots\ldots 12$$

Assuming that the thermal conductivity does not vary in the medium, the heat balance can be rewritten as the following:

$$\frac{\partial^2 T}{\partial x^2} + \frac{\partial^2 T}{\partial y^2} + \frac{\dot{Q}}{k} = \frac{1}{\alpha}\frac{\partial T}{\partial t} \ldots\ldots\ldots\ldots\ldots\ldots\ldots 13$$

where α is the thermal diffusivity defined as $\frac{k}{\rho C_p}$.

2.4 Chip Temperature Model

Considering orthogonal cutting (Fig. 4), with two-dimensional heat flow and one-dimensional mass transfer, the heat balance equation [as shown in Eq. (13)] for the discrete chip zone can be written in partial differential equation form in Cartesian coordinates as the following,

$$\left(\frac{\partial^2 T_c}{\partial x^2} + \frac{\partial^2 T_c}{\partial y^2}\right) + \frac{\dot{Q}_c}{k_c} = \left(\frac{\rho C_c}{k_c}\right).\frac{\partial T_c}{\partial t} = \left(\frac{\rho C_c}{k_c}\right).V_c\frac{\partial T_c}{\partial x} \ldots\ldots\ldots\ldots\ldots\ldots\ldots 14$$

where $\dot{Q}_c$, k_c, C_c are the energy generation rate per unit area in the differential chip zone, thermal conductivity and specific heat capacity of the chip, respectively. In the above equation, it should be noticed that $\frac{\partial T_c}{\partial t}$ can be replaced by $V_c\frac{\partial T_c}{\partial x}$. In order to solve the partial differential equation using the finite difference method, the following approximations can be made (Fig. 5),

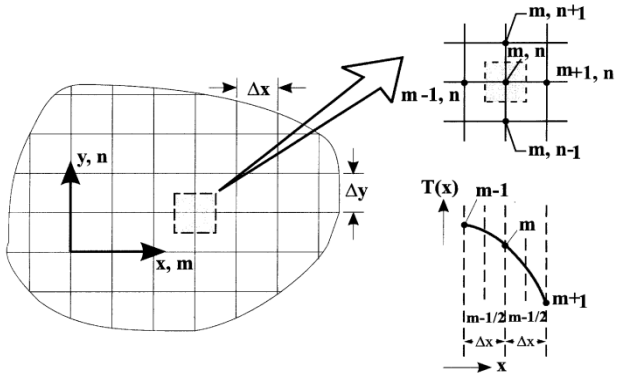

Fig. 5. Illustration of nodal network in 2-D control volume and Finite Difference Approximation

$$\left.\frac{\partial^2 T}{\partial x^2}\right|_{x,y} \simeq \frac{T_{(x+\delta x,y)} + T_{(x-\delta x,y)} - 2T_{(x,y)}}{\delta x^2}, \left.\frac{\partial^2 T}{\partial y^2}\right|_{x,y} \simeq \frac{T_{(x,y+\delta y)} + T_{(x,y-\delta y)} - 2T_{(x,y)}}{\delta y^2} \ldots\ldots\ldots\ldots 15$$

Therefore, by using the above approximations, the governing equation in the partial differential equation form (Eq. (14)) can be rewritten as in the following finite difference form:

$$\frac{T_{(x+\delta x,y)} + T_{(x-\delta x,y)} - 2T_{(x,y)}}{\delta x^2} + \frac{T_{(x,y+\delta y)} + T_{(x,y-\delta y)} - 2T_{(x,y)}}{\delta y^2} + \frac{\dot{Q}_{c(x,y)}}{k_c} = \left(\frac{\rho C_c}{k_c}\right).V_c\frac{\partial T_{c(x,y)}}{\partial x} \ldots\ldots 16$$

The chip geometry must be meshed into small discrete elements for the finite difference solution of the chip temperature field and the equilibrium equation above needs to be written for each nodal point of the chip (Fig. 4). The aspect ratio of the mesh can be unity to simplify the solution, $\delta x = \delta y$.

In the equilibrium equation (Eq. (16)), the heat flow into the differential chip control zone $(\dot{Q}_c)$ from the frictional heat source can be localized for each node along the chip–tool contact length as:

$$\dot{Q}_{c(i)} = \left.\frac{(1-\Gamma_i).\dot{Q}_f.dx}{l_{cn}}\right\} if\ and\ only\ if\ 1 \le i \le N_x + 1 \ldots\ldots\ldots\ldots\ldots\ldots\ldots 17$$

Where Γ_i represents the proportion of the frictional heat flowing into the tool at the ith nodal point and is unknown initially. $\dot{Q}_f$, l_{cn} and N_x are the frictional heat generation rate, chip–tool contact length and number of grids along the x axis, respectively. It should be noticed that a uniform heat generation was considered along the chip–tool contact length. The internal nodes (all nodes other than$1 \le i \le N_x + 1$) will physically have no heat

generation input. Therefore, $\dot{Q}_{c(i)}$ will be zero for all these nodes. Equilibrium equations for all of the nodes of the chip can be written as shown in Eq. (16), and all these equilibrium equations can be collected in a compact matrix form:

$$[A].\{T_c\} = \{C\} \dots\dots\dots\dots\dots\dots\dots\dots\dots\dots\dots\dots 18$$

Where $[A]$ is the square coefficient matrix determined from Eq. (16), $\{T_c\}$ is the chip temperature array with size of $(N_y + 1)(N_x + 1)$ (where N_y is the number of meshes along the *y* axis as shown in Fig. 4), and $\{C\}$ is the heat generation array. The temperature of each nodal point in the chip nodal network corresponds to a value in the chip temperature array, $\{T_c\}$. $\{T_c\}$ can be determined as:

$$\{T_c\} = [A]^{-1}.\{C\} \dots\dots\dots\dots\dots\dots\dots\dots\dots\dots\dots 19$$

Writing the equilibrium equation for each nodal point $\left(1 \le i \le (N_y + 1)(N_x + 1)\right)$ leads to the elements of coefficient matrix, $[A]$, and heat generation array, $\{C\}$.

2.5 Tool Temperature Model

Whereas Cartesian coordinates are used for the chip, applying polar coordinates to the tool is advantageous due to the mathematical accuracy and its convenience in the computational implementation of the model. Similar to the chip temperature model, the heat transfer equilibrium equations for the control zone around the tool nodal points can be written in the polar coordinates as,

$$\frac{\partial^2 T_t}{\partial r^2} + \frac{1}{r}\frac{\partial T_t}{\partial r} + \frac{1}{r^2}\frac{\partial^2 T_t}{\partial \psi^2} + \frac{\dot{Q}_t}{k_t} = 0 \dots\dots\dots\dots 20$$

where T_t represents the tool temperature field, *r* is the radial distance between the nodal point in concern and the tool tip shown as point O in Fig. 4, and ψ is the angular position of the nodal point. k_t and $\dot{Q}_t$ denote the tool thermal conductivity and heat generation rate per unit area in the control zone, respectively.

In order to write the above partial differential equation in the form of finite difference, the following approximations can be made:

$$\left.\frac{\partial^2 T}{\partial r^2}\right|_{r,\psi} \simeq \frac{T_{(r+\delta r,\psi)} + T_{(r-\delta r,\psi)} - 2T_{(r,\psi)}}{\delta r^2}, \left.\frac{1}{r}\frac{\partial T}{\partial r}\right|_{r,\psi} \simeq \frac{T_{(r+\delta r,\psi)} + T_{(r-\delta r,\psi)} - 2T_{(r,\psi)}}{2.r.\delta r} \dots\dots\dots\dots 21$$

$$\left.\frac{1}{r^2}\frac{\partial^2 T}{\partial r^2}\right|_{r,\psi} \simeq \frac{T_{(r,\psi+\delta\psi)} + T_{(r,\psi-\delta\psi)} - 2T_{(r,\psi)}}{r^2\delta\psi^2} \dots\dots\dots\dots 22$$

Therefore, the finite difference form of the tool heat balance equation (Eq. (20)) will be as the following;

$$\left(\frac{T_{t(r+\delta r,\psi)} + T_{t(r-\delta r,\psi)} - 2T_{t(r,\psi)}}{\delta r^2} + \frac{T_{t(r+\delta r,\psi)} + T_{t(r-\delta r,\psi)} - 2T_{t(r,\psi)}}{2r\delta r} + \frac{T_{t(r,\psi+\delta\psi)} + T_{t(r,\psi-\delta\psi)} - 2T_{t(r,\psi)}}{r^2\delta\psi^2}\right) + \frac{\dot{Q}_{t(r,\psi)}}{k_t} = 0 \dots\dots\dots\dots 23$$

The frictional heat flow rate into the tool is given by

$$\dot{Q}_{t(i)} = \left.\frac{\Gamma_i.\dot{Q}_f.dx}{l_{cn}}\right\} if\ and\ only\ if\ 1 \le i \le N_x + 1 \dots\dots\dots\dots 24$$

Similar to the chip heat balance equations, the equilibrium equations for all nodal points of the tool can be written and collected in a compact form:

$$[D].\{T_t\} = \{E\} \dots\dots\dots\dots\dots\dots\dots\dots\dots\dots\dots\dots 25$$

where $[D]$ is the square coefficient matrix determined from Eq. (23), $\{T_t\}$ is the tool temperature array, $\{E\}$is the heat generation array for the tool.

Therefore, the tool temperature distribution can be determined from

$$\{T_t\} = [D]^{-1}.\{E\} \dots\dots\dots\dots\dots\dots\dots\dots\dots\dots\dots 26$$

The finite difference equilibrium equation of the tool (Eq. (23)) needs to be written for each nodal point of the tool. Thus, the elements of the tool coefficient matrix, $[D]$, and the heat generation array, $\{E\}$, can be determined for each tool node $\left(for\ 1 \le i \le \left(N_p + 1\right)\left(\frac{r_{max}}{\delta r} + 1\right) - N_p;\right.$ where the number of discrete angles, $\left.N_p = \frac{\pi/_2 - \gamma_n - \alpha_p}{d\psi}\right)$.

In the chip and tool heat balance equations, besides the tool and chip temperature distributions, the partitions of the heat (Γ_i) at the nodal points along the chip-workpiece contact length are also not known initially. Therefore, an iterative process is required for the computation. Initial values between 0 and 1 can be assigned for the heat partitions, Γ_i, at each nodal point. The tool and chip temperature fields can be determined based on the initial assignments of Γ_i. After solving the chip and tool heat balance equations [Eq. (19) and (26)], if temperatures of the corresponding tool and chip nodal points, at which the tool and chip are in contact, are different than each other, then the heat partition value for the corresponding nodal points need to be modified. The following formulation can be employed for the partition modification,

$$d\Gamma_{(1:N_x+1)} = Gain.\frac{\left(T_{c(1:N_x+1)} - T_{t(1:N_x+1)}\right)}{\left(T_{c(1:N_x+1)} + T_{t(1:N_x+1)}\right)} \dots\dots\dots 27$$

The above equation compares the difference between the chip and tool temperatures at every nodal point, at which chip and tool is in contact, with their average temperature.

Initial value of Gain may be set to unity; if numerical divergence occurs during the solution, its value should be decreased to guarantee convergence at the cost of computation time.

If the maximum of $d\Gamma_{(1:N_x+1)}$ is greater than a certain predefined percentage, then the new heat partition values for the corresponding nodes can be assigned as

$$\Gamma_i = \Gamma_i + d\Gamma_i \; for \; 1 < i < N_x + 1 \dots\dots 28$$

With these new heat partitions, the finite difference equations for the chip and tool are solved again and $d\Gamma_{(1:N_x+1)}$ values are re-determined. The new partition should allow the temperature fields of the tool and chip at the contact region to converge. This iterative solution will continue until maximum of d $d\Gamma_{(1:N_x+1)}$ reaches to a predefined satisfactory low level. Thus, at the end of the iterative solution, the temperature fields of the tool and chip can be determined from $\{T_t\}, \{T_c\}$.

III. SIMULATION RESULTS AND DISCUSSIONS

3.1 Heat Flux And Temperature Estimation

The temperature fields are obtained from the solution of the direct problem given by Eq. (6) solved using the estimated values of the heat flux generated at chip–tool interface for each cutting condition. Figs. 6 and 7 present the heat flux and temperature estimation respectively at the chip–tool interface for the most several conditions. Figs. 6 and 7 also show the repeatability in the heat flux and temperature estimations for three similar tests of the same cutting conditions. Some dispersion of the results may be credited to the inexact chip–tool contact area, measurement errors or uncertainty in the thermal properties values.

Figs. 8 and 9 shows in detail the temperature behavior in the tool rake face plane and Fig. 10 presents the temperature varying in the tool thickness direction. According to the Figs. 10 there is a high temperature gradient in the insert. It can be observed a steep temperature drop on the tool rake face where the temperature decreases from 990°C at the tool tip to about 226°C at 2.9 mm distance from the tool tip in the insert thickness direction. It also can be observed that along the length of the interface contact the temperature decreases from 990 to 479°C at 1.2 mm or to 276°C at 2.5 mm distance from the tool tip. Fig. 8 show the level of temperature and the temperature gradient in the tool holder. For example, the temperature in the tool holder goes from 136°C at interface with the tool shim to approximately the room temperature in region exposed to the ambient air.

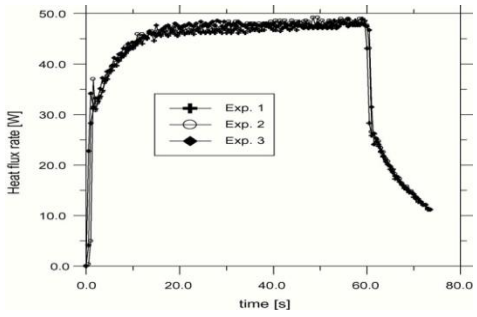

Fig. 6. Heat flux estimated at the chip–tool interface when using several cutting conditions.

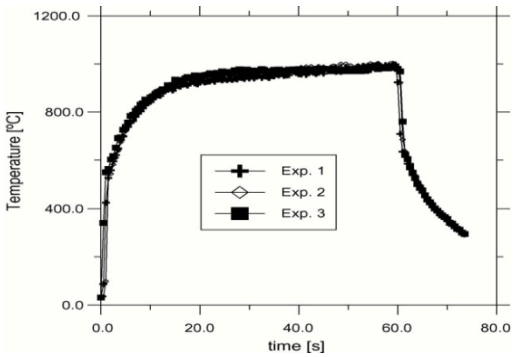

Fig. 7. Temperature estimated at the chip–tool interface when using several cutting conditions.

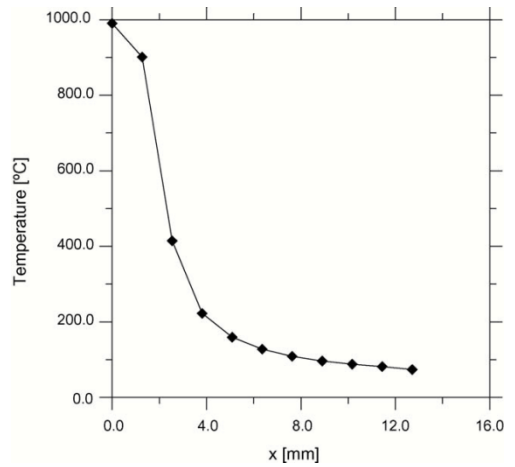

Fig. 8. Chip–tool interface temperature at 60s in the x-direction.

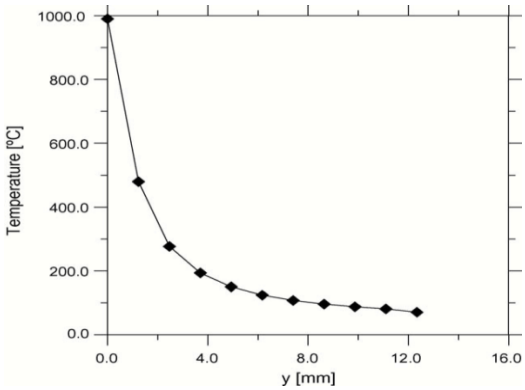

Fig. 9. Chip–tool interface temperature at 60 s in the y-direction for several cutting conditions.

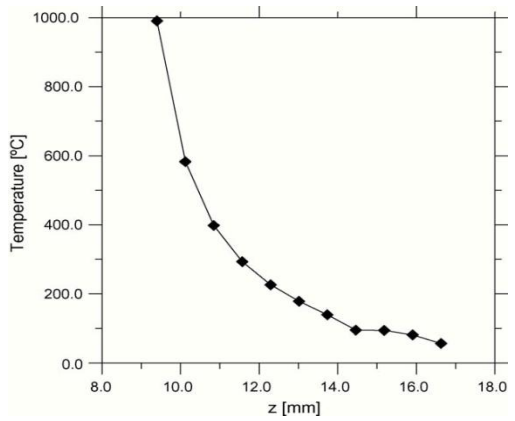

Fig. 10. Chip–tool interface temperature at 60s in the z (thickness) direction for several cutting conditions.

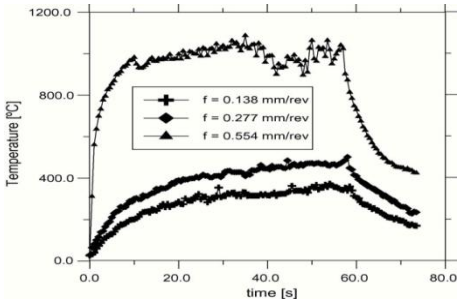

Fig. 11. Influence of feed rate in the chip–tool interface temperature for several cutting conditions.

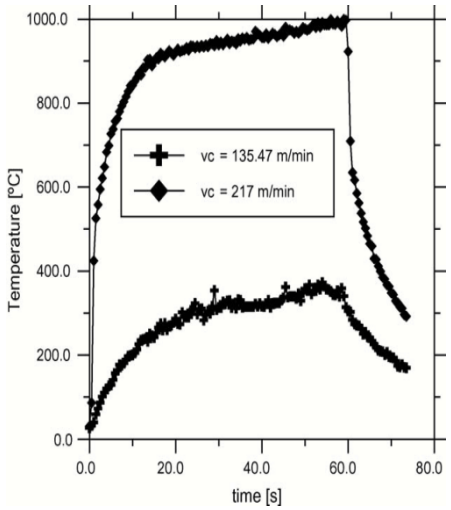

Fig, 12. Influence of cutting speed in the chip–tool interface temperature for several cutting conditions.

3.2 Influence Of Cutting Conditions In The Temperature Estimation

Figs. 11 and 12 show the behavior of the temperature against the cutting speed and the feed rate, respectively, for cemented carbide insert machining a gray cast iron workpiece. Fig. 11 reveals that the higher the cutting speed the higher the interface contact temperature. This behavior is due to the fact that as the cutting speed increases, the strain rates in primary and secondary shear zones also increase, and so does the heat flux generated. Fig. 12 presents the influence of the feed rate. Again, it can be observed that temperature increases as the feed rate increases.

3.3 Continuous Machining Tests

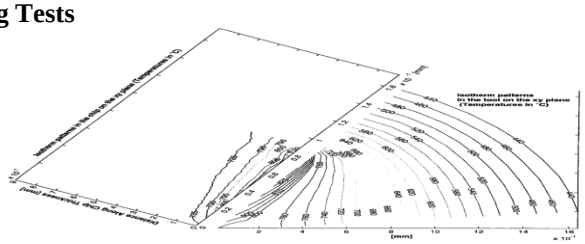

Fig. 13. Predicted isotherms patterns of the chip during the machining of mild steel under the conditions given by Boothroyd (1963) [temperatures in ^{o}C]

Boothroyd (1963) used infra-red photographic techniques to measure the temperature of a pre-heated tubular work-piece which was end-machined on a lathe. Orthogonal cutting conditions with the feed per revolution of 0.604mm/rev were performed on a mild steel tube with an outside diameter of 63.5 and 6.35 mm wall thickness. Boothroyd indicated that measurements of the width of the chip after machining did not show an increase in the width of chip exceeding 4% of the original width and the average increase was 2.2%. Due to this result, plane strain conditions could be assumed. He presented the measured isotherm patterns on the chip and on the work-

piece at a cutting speed of 22.86 m/min, a tool rake angle of 30°, and clearance angle of 7°, the pre-heating temperature of the workpiece was 611°C. The shear angle was calculated as 40.5 degrees from ratio of the given chip thicknesses using the geometric relationship.

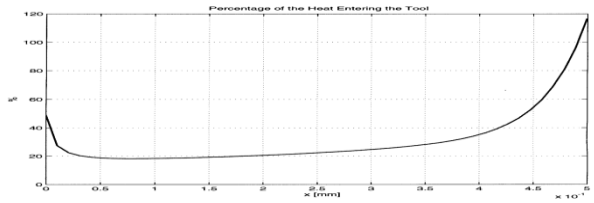

Fig. 14. Variation of the portion of heat flux that flows into the tool along the chip-tool contact region on the rake face

The temperature rise due to the shear was calculated as 169.4°C from Eq. (9). Simulation was performed for the same cutting conditions using workpiece conductivity, density and thermal capacity of 42.6 W/(m·K), 7850kg/m3, 473 J/(kg·°C), respectively, for the mild steel.

Tool conductivity, density and thermal capacity were 28.4W/(m·K), 11100kg/m3, 276J/(kg·°C), respectively. For the finite difference solution, N_y, N_p and $d\Gamma_{max}$ were set to 10, 8 and 3%, respectively.The simulated chip and tool temperature isotherm patterns are given in Fig. 13. Predicted isotherms patterns of the chip during the machining of mild steel under the conditions given by Boothroyd (1963) (temperatures in °C) measured on the rake face was around 760 °C, and the simulation results show the maximum temperature as 810°C.

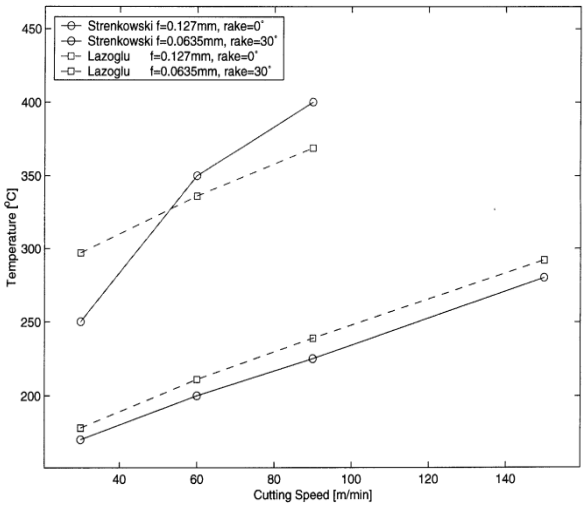

Fig. 15. Variation of average interface temperature with cutting speed and feed per revolution (Strenkowski's measured temperature vs Lazoglu & Altintas's model predictions) for A16061

The simulations show slightly higher temperature close to the shear zone (785°C) as opposed to 660°C reported by Boothroyd. The small discrepancies may be attributed to the preheating of the tube (611°C) by Boothroyd, which could have changed the properties of the mild steel workpiece. Stephenson and Ali measured temperature during the continuous and interrupted turning of Al2024-T351 tubes by using a tool–chip thermocouple method. The tool was a standard C2 WC tool. The first set of the experimental tests was performed by continuous cutting and the average measured temperature was 280 °C. In the test, cutting speed, feed per revolution, cutting force, feed force and cut chip thickness were 1.36 m/s, 0.165 mm, 573 N, 329 N and 0.333 mm. The width of cut was 2.54 mm. The rake and inclination angles were zero. Based on the previous experiments, they assumed that the chip–tool contact length was given to be 1.5 times the cut chip thickness. Simulation was performed for this cutting conditions using workpiece conductivity, density and thermal capacity of 177 W/(m·K), 2700 kg/m3, 613 J/(kg·°C), respectively, for Al2024-T351. Tool conductivity, density and thermal capacity were 28.4 W/m-K, 11100 kg/m3, 276 J/(kg·°C), respectively. The shear angle was determined from the chip ratio as 26.4 degrees. The friction angle was determined as 29.8 degrees from the measured cutting and feed force values. The temperature rise due to the shear was calculated as 215 °C from Eq. (9). For the finite difference solution, N_y, N_p and $d\Gamma_{max}$ were set to 10, 8 and 3%, respectively. The predicted steady state average temperature was found to be 283 °C, which is very close to 280 °C measured by Stephenson and Ali. The temperature fields of the chip and tool and the variation of partition of the heat flux

which flows into the tool along the chip–tool contact region on the rake face for these continuous cutting conditions are also illustrated in Figs. 13 and 14, respectively. The maximum tool temperature is predicted to be about 370 °C and it occurs at about 0.4 mm away from the cutting edge. The total chip contact length is about 0.525 mm and the uncut chip is about 0.165 mm. It is interesting to observe in Fig. 14 that close to the end of the contact region (~0.5 mm), most of the heat flux flows into the tool. Γ_i may sometimes be larger than 100%. This indicates that not only the frictional energy transferred to the tool but also some of the chip heat is transmitted to the tool in order to balance relatively cold tool backside temperature.

Strenkowski and Moon turned Al6061-T6 tubes with a high speed steel tool at different cutting speeds, feedrates and rake angles. Simulation was performed for the same cutting conditions and work material using workpiece conductivity, density and thermal capacity of 204 W/(mK), 2700 kg/m3, 896 J/(kg·°C), respectively. Tool conductivity, density and thermal capacity were 42.6 W/(m·K), 7858 kg/m3, 612 J/(kg·°C), respectively. For the case with the feed per revolution of 0.0635 mm/rev and the rake angle of 30 degrees, the shear angle, the friction angle and the temperature rise due to the shear were calculated as 28.3 degrees, 37.1 degrees and 66.5°C, respectively. For the case with the feed per revolution of 0.127 mm/rev and the rake angle of 0 degree, the shear angle, the friction angle and the temperature rise due to the shear were calculated as 21.2 degrees, 25.7 degrees and 99 °C. For the finite difference solution,N_y, N_p and $d\Gamma_{max}$ were set to 8, 8 and 5%, respectively. As seen in Fig. 15, the simulation results and experimental measurements agree well.

IV. CONCLUSIONS

The temperature field in any region of the tool set (insert, shim and tool-holder) is calculated from the heat flux estimation at the cutting interface. The determination of the temperature and of the heat flux at the chip–tool interface is done by using the inverse heat conduction problem technique. A great contribution of this work is the development of a technique that takes into account not just the insert tip but also the shim and tool holder.Heat balance equations were determined in partial differential equation forms for the chip and for the tool. The finite difference method was utilized for the solutions of the steady-state tool and chip temperature fields. The chip thickness was discretized and Steady-state chip and tool temperature fields were determined for each of these discretized machining intervals. Based on thermal properties and boundary conditions, time constants were determined for each discrete machining interval.Simulations were performed for different materials under various cutting conditions. The results for continuous machining processes agreed well with experimentally measured temperatures.The proposed algorithm can be utilized in selecting cutting speed, feed rate and tool rake and clearance angles in order to avoid excessive thermal loading of the tool, hence reducing the edge chipping and accelerated wear of the cutting tools.

REFERENCES

[1] J.V. Beck, B. Blackwell, Handbook of Numerical Heat Transfer, John Wiley & Sons Inc., New York, 1988.
[2] G. Boothroyd, Temperatures in orthogonal metal cutting, Proceedings of the Institution of Mechanical Engineers 177 (29) (1963) 789–803.
[3] S.R. Carvalho, Tool temperature estimation during cutting process, Doctorate Thesis, Federal University of Uberlˆandia, Brazil, 2005 (in Portuguese).
[4] S.R. Carvalho, S.M.M. Lima e Silva, A.R. Machado, G. Guimaraes, Temperature Determination at the Chip-Tool Interface using an inverse Thermal Model Considering the Tool and the Tool Holder, Journal of Material Processing Technology 179 (2006) 97-104.
[5] Y. Jarny, M.N. Ozisik, J.P. Bardon, A general optimization method using adjoint equation for solving multidimensional inverse heat conduction, J. Heat Mass Transfer 34 (1991) 2911–2919.
[6] T.C. Jen, G. Gutierrez, Numerical heat transfer analysis in transient cutting tool temperatures, in: Proceedings of the 34th National Heat Transfer Conference, 34 Pittsburgh/Pennsylvania, 2000.
[7] R.S. Khurmi, J. K. Gupta, Machine Design, Multi-colour edn. , S.Chand and Company Ltd, New Delhi India, 2000.
[8] F. Klocke, W. Konig, Gerschwiler, Advanced Machining of Titanium and Nickel-Based Alloys, Advanced Manufacturing Systems and Technology, Springer Verlag, New York, USA, 1996.
[9] I. Lazoglu, Y. Altintas, Prediction of tool chip temperature in continuous and interrupted machining, Int. J. Mach. Tools Manuf. 42 (2002) 1011–1022.
[10] J. Lin, Inverse estimation of the tool–work interface temperature in end milling, Int. J. Mach. Tools Manuf. 35 (1995) 751–760.
[11] E.G. Loewen, M.C. Shaw, On the Analysis of Cutting-Tool Temperatures, Transactions of ASME, Journal of Engineering for Industry 76 (1954) 217–231.
[12] A.C.A. Melo, G. Guimaraes, A.R. Machado, Evaluation of the behavior of estimated cutting temperature with the main machining parameter using inverse heat conduction, in: Proceedings of the Behavior of Materials on Machining: Opportunities and Prospects for Improved Operations, London, UK, 1999, pp. 311–320.
[13] M.M. Ohadi, K.L. Cheng, Modeling of temperature distributions in the workpiece during abrasive waterjet machining, J. Heat Transfer 115 (1998) 446–452.
[14] P.L.B. Oxley, Mechanics of Machining: An Analytical Approach to Assessing Machinability, John Wiley & Sons, New York, USA, 1989.
[15] S.V. Patankar, Numerical Heat Transfer and Fluid Flow, Hemisphere Publishing Corporation, USA, 1980.
[16] R. Radulescu, S.G. Kapoor, An analytical model for prediction of tool temperature-fields during continuous and interrupted cutting, J. Eng. Ind. 116 (1994) 135–143.

[17] H. Ren, Y. Altintas, Mechanics of machining with chamfered tools, Trans. ASME, Journal of Manufacturing and Engineering and Science 122 (2000) 650–659.
[18] X.J. Ren, Q.X. Yang, R.D. James, L. Wang, Cutting temperatures in hard turning chromium hard facings with PCBN tooling, Journal Material Processing Technology 147 (2004) 38–44.
[19] G. B. Richard, J. K. Nisbelt, Shigley's Mechanicaal Engineering Design, 8th edn, McGraw Hill, Singapore, 2008.
[20] M. Shatla, Y.C. Yen, O. Castellanos, L. Menegardo, T. Altan, T, Prediction of Cutting Forces, Temperatures and Stresses from Flow Stress Data and Cutting Conditions—Research in Progress, in: Proceedings of the Second CIRP International Workshop on Modeling of Machining Operations, Ecole Centrale De Nantes, Nantes, France, January 25-26, 1999.
[21] A.J.R. Smith, J.A. Armarego, Temperature prediction in orthogonal cutting with a finite difference approach, Annals of CIRP, 1981.
[22] D.A. Stephenson, An inverse method of investigation deformation zone temperature in metal cutting, J. Eng. Ind. 113 (1991) 129–136.
[23] D.A. Stephenson, A. Ali, Tool temperatures in interrupted metal cutting, Transactions of ASME, Journal of Engineering for Industry 114 (1992) 127–136.
[24] J.S. Strenkowski, K.J. Moon, Finite element prediction of chip geometry and tool/workpiece temperature distributions in orthogonal metal cutting, Transactions of ASME, Journal of Engineering for Industry 112 (1990) 313–318.
[25] A.A.O. Tay, A review of methods of calculating machining temperature, Journal of Material Processing Technology 36 (1993) 225–257.
[26] J. Tlusty, E. Orady, Effect of Thermal Cycling on Tool Wear in Milling, in: 9th NAMRC Conf., Penn.State University, May 1981.
[27] K.J. Trigger, B.T. Chao, An Analytical Evaluation of Metal Cutting Temperatures, Transactions of ASME 73 (1951) 57–68.
[28] E. Usui, T. Shirakashi, T. Kitagawa, Analytical prediction of three dimensional cutting process, Part 3: Cutting temperature and crater wear of carbide tool, Transactions of ASME, Journal of Engineering for Industry 100 (1978) 236–243.
[29] G.N. Vanderplaats, Design Optimization Tools, Vanderplaats Research & Development Inc., Colorado Springs, 1995.